Published August 4, 2014

−/−/− (loxP−) #1 and #2 using a pair of primers (5′-CGCAAGCTTGCGGCCATGGCGCTGCTGCG-3′ and 5′-CGCTCTAGATCAAGTGTTGTCCAGGAAGAC-3′), and then subcloned between the HindIII and XbaI sites of pcDNA3.1(+) (Invitrogen). Sequencing of the resulting plasmids revealed that gEDEM2 cDNA obtained from gEDEM2 −/−/− (loxP−) #1 and #2 was a mixture of two cDNAs designated a and b and that both contained one or two deletions, which created a stop codon in exon 5 (Fig. S1 K). Indeed, in vitro translation of the fragment did not produce any protein, whereas that of the WT fragment produced a protein of 75 kD, as expected (Fig. S1 K). We thus used −/−/− (loxP−) #1 as gEDEM2-KO (Fig. 2 A). Two independent clones (−/− #1 and #2) in which both alleles of the gEDEM3 gene were disrupted by EcoGPT and HisD or Neo-loxP were obtained (Fig. S1, H and I). As RT-PCR analysis showed that gEDEM3 mRNA was not expressed in these clones (Fig. S1 J), we used −/− #1 as gEDEM3-KO (Fig. 2 A).

Exons encoding the transmembrane domain of gERmanI were replaced with drug-resistance genes (Fig. S1 L). Two independent clones (−/− #1 and #2) in which both alleles of the gERmanI gene were disrupted by Neo-loxP and Puro-loxP were obtained (Fig. S1, M and N). As RT-PCR analysis showed that gERmanI mRNA was not expressed in these clones (Fig. S1 O), we used −/− #1 as gERmanI-KO (Fig. 2 A).

Construction of human targeting vectors

The DT-A-pA/loxP/PGK-Neo-pA/loxP vector was provided by Laboratory for Animal Resources and Genetic Engineering, Center for Developmental Biology, Institute of Physical and Chemical Research, Kobe, Japan. The puromycin- and zeocin-resistance genes were amplified from pPur (Takara Bio Inc.) and pVgRXR (Invitrogen) vectors, respectively, by PCR using the primers 5′-CGACCTGCAGCCAATATGACCGAGTACAAGCCCACGG-3′ and 5′-TTACAGCGGATCCCCTCAGGCACCGGGCTTGC-3′ and 5′-CGACCTGCAGCCAATATGGCCAAGTTGACCAGTGCC-3′ and 5′-TTACAGCGGATCCCCTCAGTCCTGCTCCTCGGCC-3′, respectively, and then inserted using the In-Fusion cloning method (Takara Bio Inc.) into the inverse PCR product of DT-A-pA/loxP/PGK-Neo-pA/loxP amplified with the primers 5′-GGGGATCCGCTGTAAGTCTGC-3′ and 5′-ATTGGCTGCAGGTCGAAAGGC-3′, resulting in obtaining DT-A-pA/loxP/PGK-Puro-pA/loxP and DT-A-pA/loxP/PGK-Zeo-pA/loxP, respectively, in which the neomycin-resistance gene was replaced with the puromycin- and zeocin-resistance genes, respectively.

Construction of hEDEM1 targeting vector

The 1.5-kb fragment of the hEDEM1 gene used for the 5′ arm was amplified by PCR from HCT116 cell genomic DNA using the primers 5′-ATAAGAATGCGGCCGCGTGCTCCTCCGGCTTGGCCTC-3′ and 5′-CCCAAGCTTCCTTATCAGAACCTAAG-3′, and then subcloned between the NotI and HindIII sites of the DT-A-pA/loxP/PGK-Neo-pA/loxP vector to create the DT-A-pA/loxP/PGK-Neo-pA/loxP-5′ arm (hEDEM1). The 1.5-kb fragment of the hEDEM1 gene used for the 3′ arm was amplified similarly using the primers 5′-GGGGTACCAAGTGTTTTCTTAGTTCCC-3′ and 5′-CCGCTCGAGCAGCCCCAGGACGAGCGCTC-3′, and then subcloned between the KpnI and XhoI sites of the DT-A-pA/loxP/PGK-Neo-pA/loxP-5′ arm (hEDEM1) to create pKO-hEDEM1-Neo, which was transfected into HCT116 cells. Approximately 100 colonies were obtained 20 d later.

Construction of hEDEM2 targeting vector

The 1.5-kb fragment of the hEDEM2 gene used for the 5′ arm was amplified by PCR from HCT116 cell genomic DNA using the primers 5′-GGGGTACCGCGCGATCCTCGCTCACTGC-3′ and 5′-CCGCTCGAGCCGGAAAGGCATAGAGCTCG-3′, and then subcloned between the KpnI and XhoI sites of the DT-A-pA/loxP/PGK-Puro-pA/loxP vector to create the DT-A-pA/loxP/PGK-Puro-pA/loxP-5′ arm (hEDEM2). The 1.5-kb fragment of the hEDEM2 gene used for the 3′ arm was amplified similarly using the primers 5′-ATAAGAATGCGGCCGCTGTGCGCGCTGCTGCCTCAG-3′ and 5′-CCCAAGCTTGGTCACTTCAAACGAGTGTAG-3′, and then subcloned between the NotI and HindIII sites of the DT-A-pA/loxP/PGK-Puro-pA/loxP-5′ arm (hEDEM2) to create pKO-hEDEM2-Puromycin, which was transfected into HCT116 cells. Approximately 100 colonies were obtained 17 d later.

Construction of hEDEM3 targeting vector

The 1.5-kb fragment of the hEDEM3 gene used for the 5′ arm was amplified by PCR from HCT116 cell genomic DNA using the primers 5′-GGGGTACCGAAAACCTTAAGGGAACACC-3′ and 5′-CCGCTCGAGCGCTGGGGAACCGGGGACCC3′, and then subcloned between the KpnI and XhoI sites of the DT-A-pA/loxP/PGK-Zeo-pA/loxP vector to create the DT-A-pA/loxP/PGK-Zeo-pA/loxP-5′ arm (hEDEM3). The 1.5-kb fragment of the hEDEM3 gene used for the 3′ arm was amplified similarly using the primers 5′-ATAAGAATGCGGCCGCAGCGCGATGGAGACTAGTGG-3′ and 5′-ATAAGAATGCGGCCGCTTTGCAATGATTTAAAGTAC-3′, and then subcloned into the NotI site of the DT-A-pA/loxP/PGK-Zeo-pA/loxP-5′ arm (hEDEM3) to create pKO-hEDEM3-Zeocin, which was transfected into HCT116 cells. Approximately 20 colonies were obtained 23 d later.

Online supplemental material

Fig. S1 shows how DT40 cells deficient in gEDEM1, gEDEM2, gEDEM3, or gERmanI are generated by homologous recombination. Fig. S2 shows characterization of high-mannose-type oligosaccharides of total glycoproteins prepared from DT40 cells of various genotypes. Fig. S3 shows characterization of HCT116 cells deficient in hEDEM1, hEDEM2, or hEDEM3 including Southern blot hybridization for confirmation of correct targeting and characterization of high-mannose-type oligosaccharides of total glycoproteins prepared from HCT116 cells of various genotypes. Online supplemental material is available at http://www.jcb.org/cgi/content/full/jcb.201404075/DC1.

We thank Ms. Kaoru Miyagawa for her technical and secretarial assistance, Ms. Yukiko Isono for her help in *N*-glycan analysis, and Dr. Elizabeth Nakajima for careful reading of this manuscript. We are grateful to Dr. Nobuko Hosokawa for providing anti-SEL1L antibody and to the Laboratory for Animal Resources and Genetic Engineering, Center for Developmental Biology, Institute of Physical and Chemical Research, Kobe, for providing the DT-A-pA/loxP/PGK-Neo-pA/loxP vector.

This work was financially supported in part by grants from the Ministry of Education, Culture, Sports, Science and Technology, Japan (19058009 and 26291040 to K. Mori, 26840065 to S. Ninagawa, 23221005 to T. Okada, 22020039 and 26102518 to Y. Kamiya, and 24249002 and 25102008 to K. Kato).

The authors declare no competing financial interests.

Submitted: 14 April 2014
Accepted: 26 June 2014

References

Aikawa, J., I. Matsuo, and Y. Ito. 2012. In vitro mannose trimming property of human ER α-1,2 mannosidase I. *Glycoconj. J.* 29:35–45. http://dx.doi.org/10.1007/s10719-011-9362-1

Avezov, E., Z. Frenkel, M. Ehrlich, A. Herscovics, and G.Z. Lederkremer. 2008. Endoplasmic reticulum (ER) mannosidase I is compartmentalized and required for *N*-glycan trimming to $Man_{5-6}GlcNAc_2$ in glycoprotein ER-associated degradation. *Mol. Biol. Cell.* 19:216–225. http://dx.doi.org/10.1091/mbc.E07-05-0505

Brodsky, J.L. 2012. Cleaning up: ER-associated degradation to the rescue. *Cell.* 151:1163–1167. http://dx.doi.org/10.1016/j.cell.2012.11.012

Clerc, S., C. Hirsch, D.M. Oggier, P. Deprez, C. Jakob, T. Sommer, and M. Aebi. 2009. Htm1 protein generates the N-glycan signal for glycoprotein degradation in the endoplasmic reticulum. *J. Cell Biol.* 184:159–172. http://dx.doi.org/10.1083/jcb.200809198

Cormier, J.H., T. Tamura, J.C. Sunryd, and D.N. Hebert. 2009. EDEM1 recognition and delivery of misfolded proteins to the SEL1L-containing ERAD complex. *Mol. Cell.* 34:627–633. http://dx.doi.org/10.1016/j.molcel.2009.05.018

Gauss, R., K. Kanehara, P. Carvalho, D.T. Ng, and M. Aebi. 2011. A complex of Pdi1p and the mannosidase Htm1p initiates clearance of unfolded glycoproteins from the endoplasmic reticulum. *Mol. Cell.* 42:782–793. http://dx.doi.org/10.1016/j.molcel.2011.04.027

Gonzalez, D.S., K. Karaveg, A.S. Vandersall-Nairn, A. Lal, and K.W. Moremen. 1999. Identification, expression, and characterization of a cDNA encoding human endoplasmic reticulum mannosidase I, the enzyme that catalyzes the first mannose trimming step in mammalian Asn-linked oligosaccharide biosynthesis. *J. Biol. Chem.* 274:21375–21386. http://dx.doi.org/10.1074/jbc.274.30.21375

Haze, K., H. Yoshida, H. Yanagi, T. Yura, and K. Mori. 1999. Mammalian transcription factor ATF6 is synthesized as a transmembrane protein and activated by proteolysis in response to endoplasmic reticulum stress. *Mol. Biol. Cell.* 10:3787–3799. http://dx.doi.org/10.1091/mbc.10.11.3787

Hirao, K., Y. Natsuka, T. Tamura, I. Wada, D. Morito, S. Natsuka, P. Romero, B. Sleno, L.O. Tremblay, A. Herscovics, et al. 2006. EDEM3, a soluble EDEM homolog, enhances glycoprotein endoplasmic reticulum-associated degradation and mannose trimming. *J. Biol. Chem.* 281:9650–9658. http://dx.doi.org/10.1074/jbc.M512191200

Published August 4, 2014

Horimoto, S., S. Ninagawa, T. Okada, H. Koba, T. Sugimoto, Y. Kamiya, K. Kato, S. Takeda, and K. Mori. 2013. The unfolded protein response transducer ATF6 represents a novel transmembrane-type endoplasmic reticulum-associated degradation substrate requiring both mannose trimming and SEL1L protein. *J. Biol. Chem.* 288:31517–31527. http://dx.doi.org/10.1074/jbc.M113.476010

Hosokawa, N., I. Wada, K. Hasegawa, T. Yorihuzi, L.O. Tremblay, A. Herscovics, and K. Nagata. 2001. A novel ER α-mannosidase-like protein accelerates ER-associated degradation. *EMBO Rep.* 2:415–422. http://dx.doi.org/10.1093/embo-reports/kve084

Hosokawa, N., L.O. Tremblay, Z. You, A. Herscovics, I. Wada, and K. Nagata. 2003. Enhancement of endoplasmic reticulum (ER) degradation of misfolded null Hong Kong α_1-antitrypsin by human ER mannosidase I. *J. Biol. Chem.* 278:26287–26294. http://dx.doi.org/10.1074/jbc.M303395200

Hosokawa, N., Y. Kamiya, and K. Kato. 2010a. The role of MRH domain-containing lectins in ERAD. *Glycobiology.* 20:651–660. http://dx.doi.org/10.1093/glycob/cwq013

Hosokawa, N., L.O. Tremblay, B. Sleno, Y. Kamiya, I. Wada, K. Nagata, K. Kato, and A. Herscovics. 2010b. EDEM1 accelerates the trimming of α1,2-linked mannose on the C branch of *N*-glycans. *Glycobiology.* 20:567–575. http://dx.doi.org/10.1093/glycob/cwq001

Joung, J.K., and J.D. Sander. 2013. TALENs: a widely applicable technology for targeted genome editing. *Nat. Rev. Mol. Cell Biol.* 14:49–55. http://dx.doi.org/10.1038/nrm3486

Kamiya, Y., D. Kamiya, K. Yamamoto, B. Nyfeler, H.P. Hauri, and K. Kato. 2008. Molecular basis of sugar recognition by the human L-type lectins ERGIC-53, VIPL, and VIP36. *J. Biol. Chem.* 283:1857–1861. http://dx.doi.org/10.1074/jbc.M709384200

Kamiya, Y., T. Satoh, and K. Kato. 2012. Molecular and structural basis for *N*-glycan-dependent determination of glycoprotein fates in cells. *Biochim. Biophys. Acta.* 1820:1327–1337. http://dx.doi.org/10.1016/j.bbagen.2011.12.017

Lipari, F., and A. Herscovics. 1999. Calcium binding to the class I α-1,2-mannosidase from *Saccharomyces cerevisiae* occurs outside the EF hand motif. *Biochemistry.* 38:1111–1118. http://dx.doi.org/10.1021/bi981643i

Mast, S.W., K. Diekman, K. Karaveg, A. Davis, R.N. Sifers, and K.W. Moremen. 2005. Human EDEM2, a novel homolog of family 47 glycosidases, is involved in ER-associated degradation of glycoproteins. *Glycobiology.* 15:421–436. http://dx.doi.org/10.1093/glycob/cwi014

Molinari, M. 2007. N-glycan structure dictates extension of protein folding or onset of disposal. *Nat. Chem. Biol.* 3:313–320. http://dx.doi.org/10.1038/nchembio880

Ninagawa, S., T. Okada, S. Takeda, and K. Mori. 2011. SEL1L is required for endoplasmic reticulum-associated degradation of misfolded luminal proteins but not transmembrane proteins in chicken DT40 cell line. *Cell Struct. Funct.* 36:187–195. http://dx.doi.org/10.1247/csf.11018

Ochiai, H., T. Miyamoto, A. Kanai, K. Hosoba, T. Sakuma, Y. Kudo, K. Asami, A. Ogawa, A. Watanabe, T. Kajii, et al. 2014. TALEN-mediated single-base-pair editing identification of an intergenic mutation upstream of *BUB1B* as causative of PCS (MVA) syndrome. *Proc. Natl. Acad. Sci. USA.* 111:1461–1466. http://dx.doi.org/10.1073/pnas.1317008111

Olivari, S., T. Cali, K.E. Salo, P. Paganetti, L.W. Ruddock, and M. Molinari. 2006. EDEM1 regulates ER-associated degradation by accelerating de-mannosylation of folding-defective polypeptides and by inhibiting their covalent aggregation. *Biochem. Biophys. Res. Commun.* 349:1278–1284. http://dx.doi.org/10.1016/j.bbrc.2006.08.186

Pan, S., S. Wang, B. Utama, L. Huang, N. Blok, M.K. Estes, K.W. Moremen, and R.N. Sifers. 2011. Golgi localization of ERManI defines spatial separation of the mammalian glycoprotein quality control system. *Mol. Biol. Cell.* 22:2810–2822. http://dx.doi.org/10.1091/mbc.E11-02-0118

Quan, E.M., Y. Kamiya, D. Kamiya, V. Denic, J. Weibezahn, K. Kato, and J.S. Weissman. 2008. Defining the glycan destruction signal for endoplasmic reticulum-associated degradation. *Mol. Cell.* 32:870–877. http://dx.doi.org/10.1016/j.molcel.2008.11.017

Ron, E., M. Shenkman, B. Groisman, Y. Izenshtein, J. Leitman, and G.Z. Lederkremer. 2011. Bypass of glycan-dependent glycoprotein delivery to ERAD by up-regulated EDEM1. *Mol. Biol. Cell.* 22:3945–3954. http://dx.doi.org/10.1091/mbc.E10-12-0944

Saeed, M., R. Suzuki, N. Watanabe, T. Masaki, M. Tomonaga, A. Muhammad, T. Kato, Y. Matsuura, H. Watanabe, T. Wakita, and T. Suzuki. 2011. Role of the endoplasmic reticulum-associated degradation (ERAD) pathway in degradation of hepatitis C virus envelope proteins and production of virus particles. *J. Biol. Chem.* 286:37264–37273. http://dx.doi.org/10.1074/jbc.M111.259085

Sakuma, T., H. Ochiai, T. Kaneko, T. Mashimo, D. Tokumasu, Y. Sakane, K. Suzuki, T. Miyamoto, N. Sakamoto, S. Matsuura, and T. Yamamoto. 2013. Repeating pattern of non-RVD variations in DNA-binding modules enhances TALEN activity. *Sci. Rep.* 3:3379. http://dx.doi.org/10.1038/srep03379

Sambrook, J., E.F. Fritsch, and T. Maniatis. 1989. Molecular Cloning: A Laboratory Manual. Cold Spring Harbor Laboratory Press, Cold Spring Harbor, NY.

Shenkman, M., B. Groisman, E. Ron, E. Avezov, L.M. Hendershot, and G.Z. Lederkremer. 2013. A shared endoplasmic reticulum-associated degradation pathway involving the EDEM1 protein for glycosylated and nonglycosylated proteins. *J. Biol. Chem.* 288:2167–2178. http://dx.doi.org/10.1074/jbc.M112.438275

Słomińska-Wojewódzka, M., A. Pawlik, I. Sokolowska, J. Antoniewicz, G. Węgrzyn, and K. Sandvig. 2014. The role of EDEM2 compared with EDEM1 in ricin transport from the endoplasmic reticulum to the cytosol. *Biochem. J.* 457:485–496. http://dx.doi.org/10.1042/BJ20130155

Smith, M.H., H.L. Ploegh, and J.S. Weissman. 2011. Road to ruin: targeting proteins for degradation in the endoplasmic reticulum. *Science.* 334:1086–1090. http://dx.doi.org/10.1126/science.1209235

Sokołowska. I., S. Wälchli, G. Węgrzyn, K. Sandvig, and M. Słomińska-Wojewódzka. 2011. A single point mutation in ricin A-chain increases toxin degradation and inhibits EDEM1-dependent ER retrotranslocation. *Biochem. J.* 436:371–385. http://dx.doi.org/10.1042/BJ20101493

Takahashi, N., and K. Kato. 2003. GALAXY (glycoanalysis by the three axes of MS and chromatography): a web application that assists structural analyses of *N*-glycans. *Trends in Glycoscience and Glycotechnology.* 15:235–251. http://dx.doi.org/10.4052/tigg.15.235

Tamura, T., J.C. Sunryd, and D.N. Hebert. 2010. Sorting things out through endoplasmic reticulum quality control. *Mol. Membr. Biol.* 27:412–427. http://dx.doi.org/10.3109/09687688.2010.495354

Tomiya, N., Y.C. Lee, T. Yoshida, Y. Wada, J. Awaya, M. Kurono, and N. Takahashi. 1991. Calculated two-dimensional sugar map of pyridylaminated oligosaccharides: elucidation of the jack bean α-mannosidase digestion pathway of $Man_9GlcNAc_2$. *Anal. Biochem.* 193:90–100. http://dx.doi.org/10.1016/0003-2697(91)90047-W

Tremblay, L.O., and A. Herscovics. 1999. Cloning and expression of a specific human α1,2-mannosidase that trims $Man_9GlcNAc_2$ to $Man_8GlcNAc_2$ isomer B during *N*-glycan biosynthesis. *Glycobiology.* 9:1073–1078. http://dx.doi.org/10.1093/glycob/9.10.1073

Xie, W., and D.T. Ng. 2010. ERAD substrate recognition in budding yeast. *Semin. Cell Dev. Biol.* 21:533–539. http://dx.doi.org/10.1016/j.semcdb.2010.02.007

Yoshida, H., T. Matsui, N. Hosokawa, R.J. Kaufman, K. Nagata, and K. Mori. 2003. A time-dependent phase shift in the mammalian unfolded protein response. *Dev. Cell.* 4:265–271. http://dx.doi.org/10.1016/S1534-5807(03)00022-4

SCIENTIFIC REPORTS

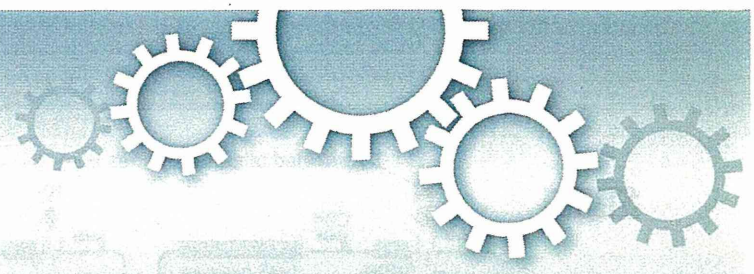

OPEN

SUBJECT AREAS:
BIOTECHNOLOGY
GENETIC ENGINEERING

Received
4 April 2014

Accepted
3 June 2014

Published
23 June 2014

Correspondence and requests for materials should be addressed to T.S. (tetsushi-sakuma@hiroshima-u.ac.jp) or T.Y. (tybig@hiroshima-u.ac.jp)

Multiplex genome engineering in human cells using all-in-one CRISPR/Cas9 vector system

Tetsushi Sakuma[1], Ayami Nishikawa[1], Satoshi Kume[1], Kazuaki Chayama[2] & Takashi Yamamoto[1]

[1]Department of Mathematical and Life Sciences, Graduate School of Science, Hiroshima University, Hiroshima 739-8526, Japan, [2]Department of Gastroenterology and Metabolism, Graduate School of Biomedical and Health Sciences, Hiroshima University, Hiroshima 734-8551, Japan.

CRISPR/Cas9-mediated genome editing is a next-generation strategy for genetic modifications, not only for single gene targeting, but also for multiple targeted mutagenesis. To make the most of the multiplexity of CRISPR/Cas9, we established a system for constructing all-in-one expression vectors containing multiple guide RNA expression cassettes and a Cas9 nuclease/nickase expression cassette. We further demonstrated successful examples of multiple targeting including chromosomal deletions in human cells using the all-in-one CRISPR/Cas9 vectors constructed with our novel system. Our system provides an efficient targeting strategy for multiplex genome/epigenome editing, simultaneous activation/repression of multiple genes, and beyond.

Genome editing using clustered regularly-interspaced short palindromic repeats (CRISPR)/Cas9 is an easy and efficient strategy for the generation of gene-modified cells and organisms[1,2]. The CRISPR/Cas9 system consists of two components: Cas9 protein and guide RNA (gRNA). The natural Cas9 protein possesses a nuclease activity and can induce a DNA double-strand break (DSB) in any genomic sequence guided by a gRNA, provided that a protospacer adjacent motif (PAM) sequence exists in the target locus[3–5]. *Streptococcus pyogenes* Cas9 (SpCas9) has been the most widely used Cas9 protein, and its PAM sequence is 5′-NGG-3′, which is the only restriction for designing CRISPR/Cas9 target sequences[6].

Since Cas9 has no DNA recognition specificity except for the PAM sequence, simple multiplication of gRNAs along with a common Cas9 protein results in multiplex genome engineering. Currently, two or more kinds of plasmids or DNA fragments are generally used for multiple targeting in cultured cells[7]. However, cotransfection of multiple plasmids can cause low targeting efficiency in cells that are inefficient in DNA transfection.

Here, we report an easy and efficient construction system for all-in-one CRISPR/Cas9 vectors expressing Cas9 protein and up to seven gRNAs. The expression cassettes of the gRNAs are tandemly ligated into a single vector using the Golden Gate cloning method. Furthermore, we demonstrate simultaneous multiple targeted mutagenesis and chromosomal deletions mediated by not only Cas9 nuclease, but also Cas9 nickase. In Cas9 nuclease-mediated genome editing, we constructed an all-in-one vector expressing Cas9 nuclease and seven gRNAs, and targeted seven genomic loci. In Cas9 nickase-mediated genome editing, we constructed an all-in-one vector expressing Cas9 nickase and six gRNAs, and targeted three genomic loci.

Results

Establishment of an all-in-one vector construction system for CRISPR/Cas9-mediated multiplex genome engineering. To establish an all-in-one vector system, we modified the pX330 vector, originally developed by the Feng Zhang laboratory[4,8], containing a single gRNA expression cassette and a Cas9 nuclease expression cassette. The protocol for inserting a gRNA-targeting sequence was the same as described in a previous paper[8] (Figure 1, STEP 1). For the assembly of gRNA cassettes, we applied the Golden Gate cloning method, which has been well-established for modular assembly of DNA-binding repeats of transcription activator-like effector nucleases (TALENs) (Figure 1, STEP 2). After assembling the plasmids, we were able to easily screen for correctly-assembled clones by colony PCR, as shown in Supplementary Fig. S1. In addition, the plasmids for the second-step reaction retained the structure of a CRISPR/Cas9 expression vector harboring single gRNA and Cas9 expression cassettes, and can therefore be used separately for single gene targeting. In this study, we

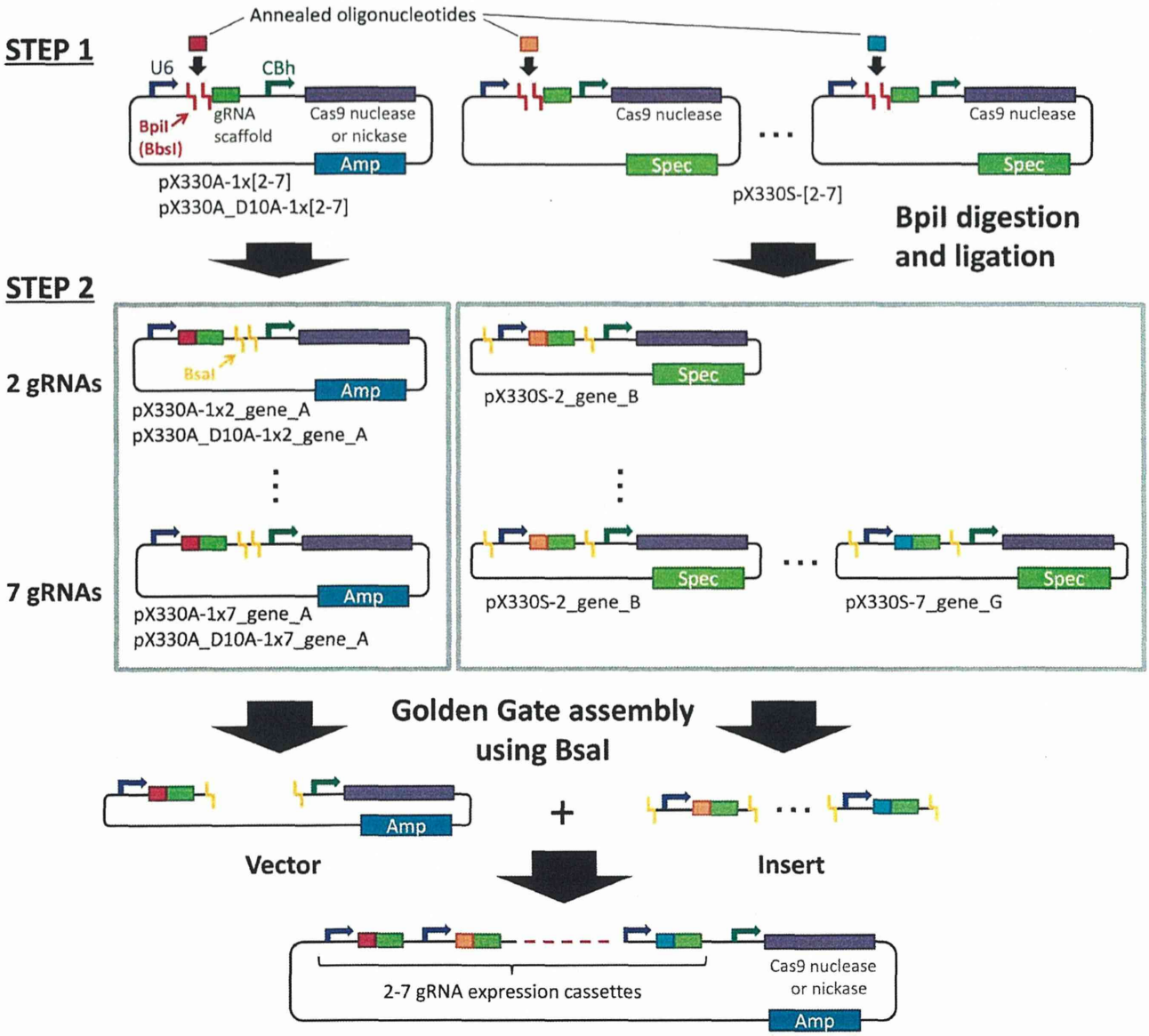

Figure 1 | Schematic overview of the all-in-one CRISPR/Cas9 vector construction system for multiplex genome engineering. Oligonucleotides corresponding to each target sequence are annealed and inserted into BpiI-digested pX330A or pX330S vectors (STEP 1). The constructed vectors harboring single gRNA expression cassettes are then assembled into an all-in-one vector harboring multiple gRNA cassettes using the Golden Gate assembly method (STEP 2). Amp, ampicillin; Spec, spectinomycin; U6, human U6 promoter; CBh, chicken beta-actin short promoter.

constructed plasmids to create all-in-one vectors expressing two to seven gRNAs with Cas9 nuclease or nickase (Figure 1).

Multiplex genome engineering with a single vector expressing seven gRNAs and one Cas9 nuclease. To prove the functionality of the all-in-one vectors created by our system, we constructed a CRISPR/Cas9 vector targeting seven genomic loci (Supplementary Fig. S2A). Oligonucleotides targeting these seven loci were synthesized and inserted separately into pX330A/S vectors. The constructed vectors were then assembled using Golden Gate cloning, resulting in an all-in-one CRISPR/Cas9 vector expressing Cas9 nuclease and seven gRNAs targeting different genomic loci (Figure 2A).

The genome editing efficiency of this multiplex CRISPR/Cas9-nuclease vector was verified using a mismatch-sensitive endonuclease assay[9]. We transfected the all-in-one vector containing seven gRNA cassettes as well as single gRNA-expressing vectors into HEK293T cells, and performed genomic PCR followed by an endonuclease cleavage assay. The results indicated that the seven gRNA-expressing all-in-one vector was able to induce mutations at almost the same level of genome editing efficiency as the single gRNA-expressing vectors (Figure 2B). Therefore, we confirmed the usefulness of our newly-established all-in-one CRISPR/Cas9-nuclease vector system.

Multiplex genome engineering with a single vector expressing six gRNAs and one Cas9 nickase. Recent progress in CRISPR/Cas9-mediated genome engineering has permitted Cas9 nickase-mediated mutagenesis[10–12]. A DSB was reported to be introduced when two gRNAs induce adjacent nicks at both DNA strands. We thus applied this paired nickase strategy to our all-in-one vector system. Since two gRNAs are required for a single locus in nickase-mediated

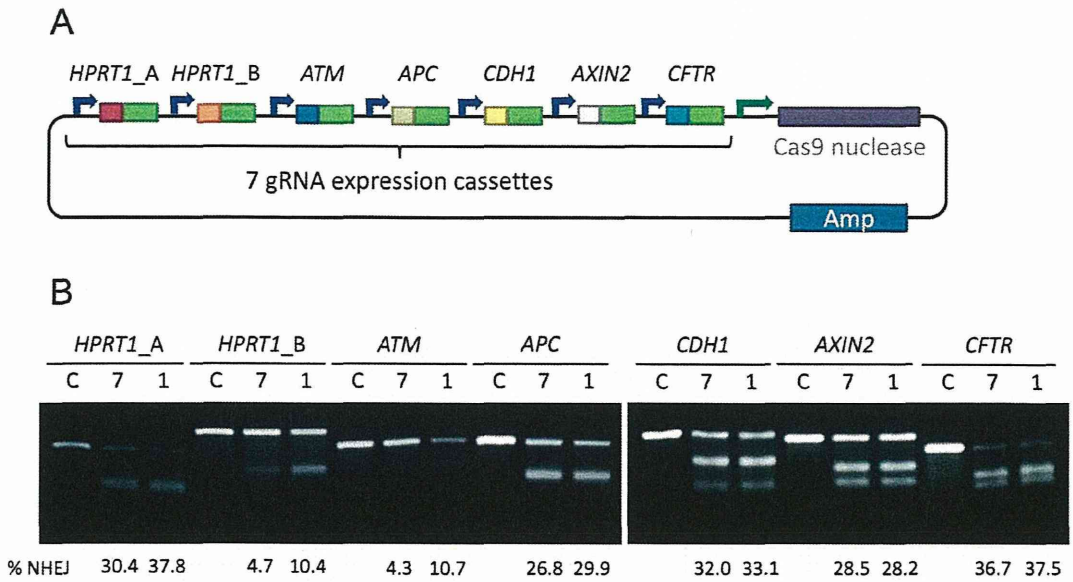

Figure 2 | Multiplex genome editing with Cas9 nuclease and seven gRNAs. (A) Schematic illustration of the all-in-one vector expressing seven gRNAs targeting seven different genomic loci and Cas9 nuclease. The blue and green bent arrows indicate the U6 and CBh promoters, respectively. (B) Genomic cleavage analysis of the seven genomic loci targeted with the all-in-one CRISPR/Cas9-nuclease vector. The products from untransfected control cells (C) and cells transfected with CRISPR/Cas9-nuclease vectors targeting seven (7) and single (1) loci were analyzed by agarose gel electrophoresis. The percentage of non-homologous end-joining (% NHEJ) was estimated using ImageJ software as previously described[30].

mutagenesis, up to three loci can be simultaneously targeted using our all-in-one vector containing six gRNA expression cassettes and one Cas9 nickase expression cassette.

We constructed an all-in-one CRISPR/Cas9-nickase vector expressing six gRNAs targeting three loci in the adenomatous polyposis coli (*APC*) gene (Figure 3A). Since the offset lengths of the individual loci were five, eight, and four base pairs, we named these loci off-5, off-8, and off-4, respectively (Supplementary Fig. S2B). The all-in-one CRISPR/Cas9-nickase vector targeting these three loci was transfected into HEK293T cells and an endonuclease cleavage assay was performed. The sizes of PCR products and cleaved fragments were nearly identical among the three loci (Figure 3B). As a result of the cleavage assay, cleaved products certainly appeared and the applicability of our all-in-one vector system for Cas9-nickase-mediated multiplex genome engineering was demonstrated (Figure 3C).

Induction of chromosomal deletions using all-in-one CRISPR/Cas9-nuclease and CRISPR/Cas9-nickase vectors. Simultaneous introduction of DSBs on the same chromosome often causes a large deletion[4,8]. To verify the applicability of our system for such chromosomal deletions, we analyzed whether the constructed all-in-one CRISPR/Cas9-nuclease and CRISPR/Cas9-nickase vectors can generate large deletions. The CRISPR/Cas9-nuclease vector, illustrated in Figure 1A, can induce two DSBs at the *HPRT1* locus, possibly resulting in ~1.9-kb deletion (Figure 4A). The CRISPR/Cas9-nickase vector, illustrated in Figure 3A, can induce two DSBs at the *APC* locus, possibly resulting in ~2.5-kb deletion (Figure 4B). Therefore, we performed genomic PCR using primers running from both outsides of DSB-inducing sites, and found that chromosomal deletions occurred at the both loci (Figure 4C). Interestingly, DNA sequencing revealed that Cas9 nuclease-mediated large deletion was likely to be repaired mainly by microhomology-mediated end-joining, resulting in the same sequence pattern, whereas Cas9 nickase-mediated large deletion resulted in a variety of sequence patterns, supposedly caused by non-homologous end-joining (Figure 4D). These differences might be due to the different DSB-inducing manner via Cas9 nuclease and Cas9 nickase. Cas9 nuclease are known to induce blunt end, while double nicking via Cas9 nickase generates protruding end[10,11].

Discussion

Multiplex genome engineering is one of the most attractive applications of the CRISPR/Cas9 system. Our study provides a simple and efficient strategy for single vector-mediated multiple targeting of up to seven genomic loci, which has not been reported to date. One matter for concern in CRISPR/Cas9-mediated multiplex genome editing is targeting specificity. Several reports have described high frequencies of off-target mutations using the CRISPR/Cas9-nuclease system[13–15]. However, recent improvements with a paired nickase strategy were reported to reduce off-target mutations dramatically[10–12]. Since we have shown the applicability of our all-in-one vector system with Cas9 nickase, our system should minimize the risk of off-target mutations in CRISPR/Cas9-mediated multiple gene targeting.

Thus far, we have only demonstrated the functionality of our all-in-one CRISPR/Cas9-nuclease and CRISPR/Cas9-nickase vectors in cultured cells. However, it should also be possible to apply these vectors directly, even in animal embryos, because Mashiko and colleagues reported that a pX330-based CRISPR/Cas9 plasmid could be directly injected for genome editing in mice[16,17], and CRISPR/Cas9 paired nickases were successfully applied for mouse genome editing in recent studies[18–20]. In addition, CRISPR/Cas9 system has been utilized in viral vectors such as lentiviral vectors[21]. Since our multiple-guided CRISPR/Cas9-nuclease and CRISPR/Cas9-nickase system will make it convenient to deliver multiple gRNA cassettes into viral vectors, it is possible that efficient viral vector-mediated multiplex genome engineering can be performed by using our system.

In addition to the genome editing approaches described above, our system is expected to be utilized in other CRISPR/Cas9-based technologies such as transcriptional control[22–24], epigenome editing[25], and visualization of specific genomic loci[26]. As simple replacement of Cas9 nuclease/nickase with inactivated Cas9 with or without various effector domains allows our system to be applied to such a wide range of applications, we anticipate that our report will provide

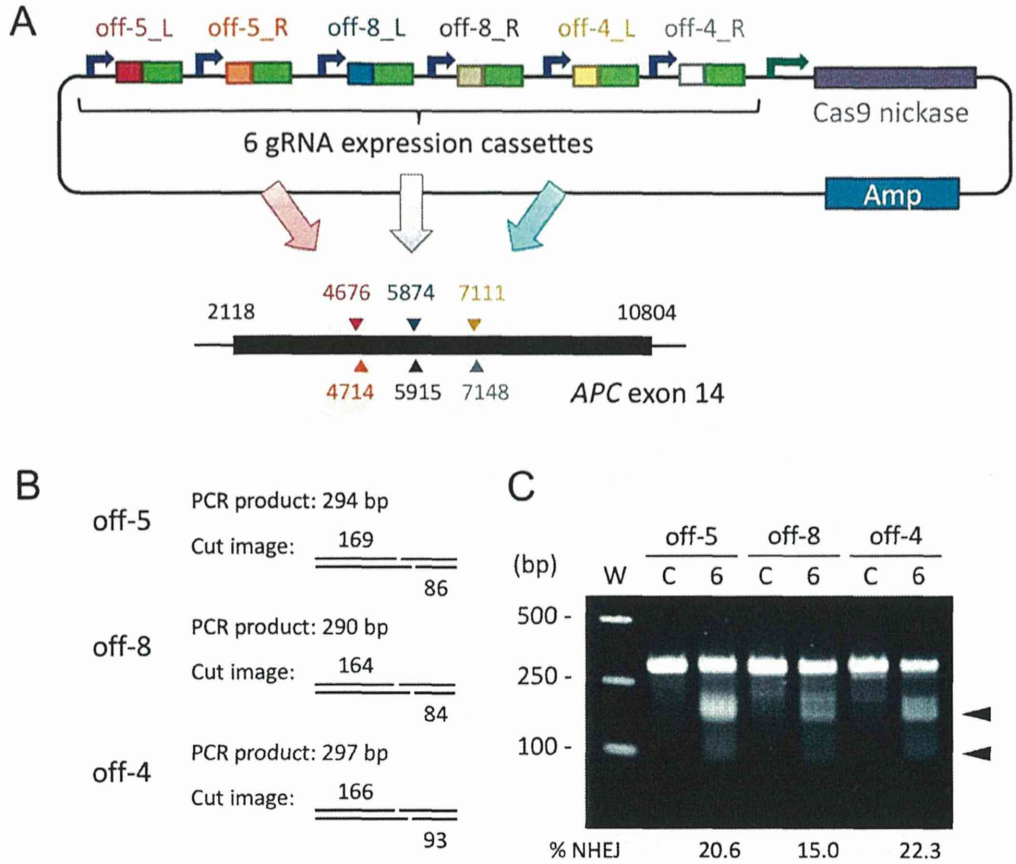

Figure 3 | Multiplex genome editing with Cas9 nickase and six gRNAs. (A) Schematic illustration of the all-in-one vector expressing six gRNAs targeting three different genomic loci and Cas9 nuclease. The black box indicates exon 14 of the human *APC* gene. The numbers from 2118 to 10804 represent the base positions in the *APC* gene transcript (NCBI reference sequence: NM_001127511.2). (B) The sizes of PCR products and cut images in each locus. (C) Genomic cleavage analysis of the three genomic loci targeted with the all-in-one CRISPR/Cas9-nickase vector. The products from untransfected control cells (C) and cells transfected with the CRISPR/Cas9-nickase vector expressing six gRNAs (6) were analyzed by agarose gel electrophoresis. The arrowheads indicate the approximate positions of the cleaved fragments. % NHEJ was estimated using ImageJ software as previously described[30]. W, Wide-Range DNA Ladder (100–2,000 bp) (Takara Bio, Shiga, Japan).

substantial contributions to a large number of researchers interested in innovative CRISPR/Cas9-based technologies.

Methods

Plasmids for the multiplex CRISPR/Cas9 vector system. All plasmids for the multiplex CRISPR/Cas9 vector system were constructed using the In-Fusion cloning method with PCR products from pX330 (Addgene, Cambridge, MA; Plasmid 42230)[4,8] and pFUS_A30A (Addgene; Plasmid 31029)[27] as summarized in Supplementary Table S1.

Insertion of annealed oligonucleotides into pX330A and pX330S vectors. To construct CRISPR/Cas9 plasmids targeting human genes, sense and antisense oligonucleotides were synthesized and annealed in the following buffer: 40 mM Tris-HCl (pH 8.0), 20 mM $MgCl_2$, and 50 mM NaCl. The annealed oligonucleotides, pX330A/S vectors, BpiI enzyme (Thermo Scientific, Rockford, IL), and Quick ligase (New England Biolabs, Beverly, MA) were mixed in a single tube with T4 DNA ligase buffer (New England Biolabs), and subjected to a thermal cycling reaction as follows: 3 cycles of 37°C for 5 min and 16°C for 10 min. After the cycling reaction, additional BpiI digestion was performed at 37°C for 1 h. A list of the constructed plasmids with the vectors used and oligonucleotide sequences is shown in Supplementary Table S2.

Golden Gate assembly and screening by colony PCR. Golden Gate assembly was performed as described previously[27–29] with some modifications. pX330A/S plasmids, BsaI-HF enzyme (New England Biolabs), and Quick ligase were mixed in a single tube with T4 DNA ligase buffer, and subjected to a thermal cycling reaction as follows: 6–15 cycles of 37°C for 5 min and 16°C for 10 min. After the cycling reaction, additional BsaI-HF digestion was performed at 50°C for 30 min. For construction of the CRISPR/Cas9-nuclease vector targeting seven genomic loci, pX330A-1x7_*HPRT1*_A, pX330S-2_*HPRT1*_B, pX330S-3_*ATM*, pX330S-4_*APC*, pX330S-5_*CDH1*, pX330S-6_*AXIN2*, and pX330S-7_*CFTR* were unified into a single vector.

For construction of the CRISPR/Cas9-nickase vector targeting three genomic loci, pX330A_D10A-1x6_off-5_L, pX330S-2_off-5_R, pX330S-3_off-8_L, pX330S-4_off-8_R, pX330S-5_off-4_L, and pX330S-6_off-4_R were unified into a single vector.

Correctly-assembled clones were screened by colony PCR using CRISPR-step2-F (5′-GCCTTTTGCTGGCCTTTTGCTC-3′) and CRISPR-step2-R (5′-CGGGCCATTTACCGTAAGTTATGTAACG-3′) primers, followed by agarose gel electrophoresis and ethidium bromide staining.

Cell culture and transfection. HEK293T cells were cultured in DMEM supplemented with 10% fetal bovine serum. Transfection of plasmids was carried out as described previously[29]. Briefly, 30,000 HEK293T cells were transfected with 400 ng of CRISPR/Cas9 plasmids using Lipofectamine LTX (Life Technologies, Carlsbad, CA) in a 96-well plate. At 48 h post-transfection, the cells were collected into PCR tubes.

Cell lysis, genomic PCR, and cleavage assay. Cell lysis, genomic PCR, and detection of cleavage were conducted using a GeneArt Genomic Cleavage Detection Kit (Life Technologies) according to the manufacturer's instructions except that DNA polymerase used in the experiment of Figure 3C was KOD FX Neo (Toyobo, Osaka, Japan) instead of AmpliTaq Gold 360. Briefly, 20 μl of cell lysis buffer and 0.8 μl of protein degrader were added to cell pellets prepared as described above. After an initial program in a thermal cycler (68°C for 15 min and 95°C for 10 min), genomic PCR was carried out using 1–2 μl of cell lysates and the primers listed in Supplementary Table S3. The PCR products were subjected to re-annealing and a cleavage assay according to the manufacturer's instructions. The products were then analyzed by electrophoresis in 3% agarose gels and ethidium bromide staining.

Detection and sequencing of chromosomally deleted alleles. Chromosomally deleted alleles were detected by genomic PCR using the primers listed in Supplementary Table S4, followed by agarose gel electrophoresis and ethidium bromide staining. The deleted PCR products were then cloned into TA cloning vector using a TArget Clone -Plus- Kit (Toyobo). Sequencing was performed using an ABI

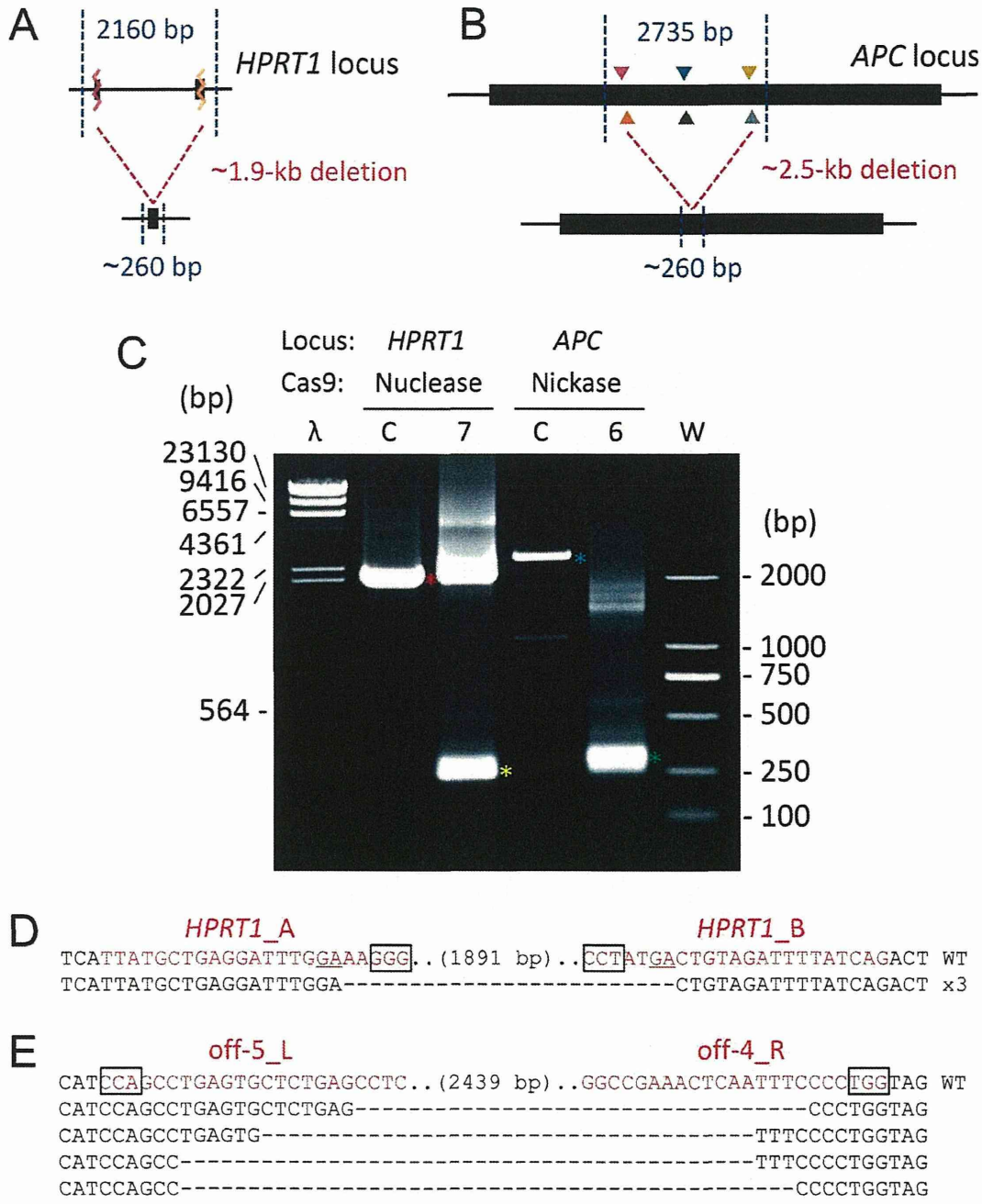

Figure 4 | Large deletions mediated by all-in-one CRISPR/Cas9 vectors. (A) Schematic illustration of large deletion at the *HPRT1* locus. The black boxes indicate exons. The blue lines and letters indicate PCR products. The zigzag lines indicate the *HPRT1*_A and *HPRT1*_B target sites. (B) Schematic illustration of large deletion at the *APC* locus. The black boxes indicate exons. The blue lines and letters indicate PCR products. The triangles indicate the off-5, off-8 and off-4 target sites. (C) Genomic PCR analysis of the *HPRT1* and *APC* loci. The products from untransfected control cells (C) and cells transfected with the CRISPR/Cas9-nuclease vector expressing seven gRNAs (7) or the CRISPR/Cas9-nickase vector expressing six gRNAs (6) were analyzed by agarose gel electrophoresis. Red and blue asterisks indicate PCR products from un-deleted alleles, whereas yellow and green asterisks indicate PCR products from chromosomally deleted alleles. λ, λHindIII marker. W, Wide-Range DNA Ladder (100–2,000 bp) (Takara Bio). (D) Sequences of the PCR products from deleted alleles at the *HPRT1* locus. The *HPRT1*_A and *HPRT1*_B target sites are indicated by red letters. PAM sites are indicated by black boxes. Deletions are indicated by dashes. (E) Sequences of the PCR products from deleted alleles at the *APC* locus. The off-5_L and off-4_R target sites are indicated by red letters. PAM sites are indicated by black boxes. Deletions are indicated by dashes.

3131xl Genetic analyzer (Life Technologies) with a BigDye Terminator v3.1 Cycle Sequencing Kit (Life Technologies).

1. Sakuma, T. & Woltjen, K. Nuclease-mediated genome editing: At the front-line of functional genomics technology. *Dev. Growth Differ.* **56**, 2–13 (2014).
2. Carroll, D. Genome engineering with targetable nucleases. *Annu. Rev. Biochem.* **83**, 409–439 (2014).
3. Jinek, M. *et al.* A programmable dual-RNA-guided DNA endonuclease in adaptive bacterial immunity. *Science* **337**, 816–821 (2012).
4. Cong, L. *et al.* Multiplex genome engineering using CRISPR/Cas systems. *Science* **339**, 819–823 (2013).

5. Mali, P. *et al.* RNA-guided human genome engineering via Cas9. *Science* **339**, 823–826 (2013).
6. Sander, J. D. & Joung, J. K. CRISPR-Cas systems for editing, regulating and targeting genomes. *Nat. Biotechnol.* **32**, 347–355 (2014).
7. Wang, H. *et al.* One-step generation of mice carrying mutations in multiple genes by CRISPR/Cas-mediated genome engineering. *Cell* **153**, 910–918 (2013).
8. Ran, F. A. *et al.* Genome engineering using the CRISPR-Cas9 system. *Nat. Protoc.* **8**, 2281–2308 (2013).
9. Guschin, D. Y. *et al.* A rapid and general assay for monitoring endogenous gene modification. *Methods Mol. Biol.* **649**, 247–256 (2010).
10. Mali, P. *et al.* CAS9 transcriptional activators for target specificity screening and paired nickases for cooperative genome engineering. *Nat. Biotechnol.* **31**, 833–838 (2013).
11. Ran, F. A. *et al.* Double nicking by RNA-guided CRISPR Cas9 for enhanced genome editing specificity. *Cell* **154**, 1380–1389 (2013).
12. Cho, S. W. *et al.* Analysis of off-target effects of CRISPR/Cas-derived RNA-guided endonucleases and nickases. *Genome Res.* **24**, 132–141 (2014).
13. Fu, Y. *et al.* High-frequency off-target mutagenesis induced by CRISPR-Cas nucleases in human cells. *Nat. Biotechnol.* **31**, 822–826 (2013).
14. Hsu, P. D. *et al.* DNA targeting specificity of RNA-guided Cas9 nucleases. *Nat. Biotechnol.* **31**, 827–832 (2013).
15. Pattanayak, V. *et al.* High-throughput profiling of off-target DNA cleavage reveals RNA-programmed Cas9 nuclease specificity. *Nat. Biotechnol.* **31**, 839–843 (2013).
16. Mashiko, D. *et al.* Generation of mutant mice by pronuclear injection of circular plasmid expressing Cas9 and single guided RNA. *Sci. Rep.* **3**, 3355 (2013).
17. Mashiko, D. *et al.* Feasibility for a large scale mouse mutagenesis by injecting CRISPR/Cas plasmid into zygotes. *Dev. Growth Differ.* **56**, 122–129 (2014).
18. Fujii, W., Onuma, A., Sugiura, K. & Naito, K. Efficient generation of genome-modified mice via offset-nicking by CRISPR/Cas system. *Biochem. Biophys. Res. Commun.* **445**, 791–794 (2014).
19. Zhou, J. *et al.* Dual sgRNAs facilitate CRISPR/Cas9-mediated mouse genome targeting. *FEBS J.* **281**, 1717–1725 (2014).
20. Shen, B. *et al.* Efficient genome modification by CRISPR-Cas9 nickase with minimal off-target effects. *Nat. Methods* **11**, 399–402 (2014).
21. Malina, A. *et al.* Repurposing CRISPR/Cas9 for in situ functional assays. *Genes Dev.* **27**, 2602–2614 (2013).
22. Qi, L. S. *et al.* Repurposing CRISPR as an RNA-guided platform for sequence-specific control of gene expression. *Cell* **152**, 1173–1183 (2013).
23. Gilbert, L. A. *et al.* CRISPR-mediated modular RNA-guided regulation of transcription in eukaryotes. *Cell* **154**, 442–451 (2013).
24. Cheng, A. W. *et al.* Multiplexed activation of endogenous genes by CRISPR-on, an RNA-guided transcriptional activator system. *Cell Res.* **23**, 1163–1171 (2013).
25. Rusk, N. CRISPRs and epigenome editing. *Nat. Methods* **11**, 28 (2014).
26. Chen, B. *et al.* Dynamic imaging of genomic loci in living human cells by an optimized CRISPR/Cas system. *Cell* **155**, 1479–1491 (2013).
27. Cermak, T. *et al.* Efficient design and assembly of custom TALEN and other TAL effector-based constructs for DNA targeting. *Nucleic Acids Res.* **39**, e82 (2011).
28. Sakuma, T. *et al.* Efficient TALEN construction and evaluation methods for human cell and animal applications. *Genes Cells* **18**, 315–326 (2013).
29. Sakuma, T. *et al.* Repeating pattern of non-RVD variations in DNA-binding modules enhances TALEN activity. *Sci. Rep.* **3**, 3379 (2013).
30. Hansen, K. *et al.* Genome editing with CompoZr custom zinc finger nucleases (ZFNs). *J. Vis. Exp.* e3304 (2012).

Acknowledgments

We are grateful to Dr Feng Zhang (Massachusetts Institute of Technology, Cambridge, MA) and Dr Daniel Voytas (University of Minnesota, Minneapolis, MN) for supplying the pX330 and pFUS_A30A plasmids, respectively. This study was supported by KAKENHI (25890014) to T.S. from the Japan Society for the Promotion of Science.

Author contributions

T.S. designed the work, performed the experiments, and wrote the manuscript. A.N. supported the creation of CRISPR/Cas9 vectors. S.K. supported human cell experiments. K.C. provided instructions. T.Y. supervised the work. All authors reviewed the manuscript.

Additional information

Supplementary information accompanies this paper at http://www.nature.com/scientificreports

Competing financial interests: The authors declare no competing financial interests.

How to cite this article: Sakuma, T., Nishikawa, A., Kume, S., Chayama, K. & Yamamoto, T. Multiplex genome engineering in human cells using all-in-one CRISPR/Cas9 vector system. *Sci. Rep.* **4**, 5400; DOI:10.1038/srep05400 (2014).

frontiers in
GENETICS

REVIEW ARTICLE
published: 29 January 2015
doi: 10.3389/fgene.2015.00010

Werner Syndrome-specific induced pluripotent stem cells: recovery of telomere function by reprogramming

Akira Shimamoto[1]*, Koutaro Yokote[2] and Hidetoshi Tahara[1]

[1] *Department of Cellular and Molecular Biology, Graduate School of Biomedical and Health Sciences, Hiroshima University, Hiroshima, Japan*
[2] *Department of Clinical Cell Biology and Medicine, Graduate School of Medicine, Chiba University, Chiba, Japan*

Edited by:
Fumiaki Uchiumi, Tokyo University of Science, Japan

Reviewed by:
Antonella Sgura, Roma Tre University, Italy
In-Hyun Park, Yale University, USA

****Correspondence:***
Akira Shimamoto, Department of Cellular and Molecular Biology, Graduate School of Biomedical and Health Sciences, Hiroshima University, 1-2-3 Kasumi, Minami-ku, Hiroshima 734-8553, Japan
e-mail: shim@hiroshima-u.ac.jp

Werner syndrome (WS) is a rare human autosomal recessive premature aging disorder characterized by early onset of aging-associated diseases, chromosomal instability, and cancer predisposition. The function of the DNA helicase encoded by WRN, the gene responsible for WS, has been studied extensively. WRN helicase is involved in the maintenance of chromosome integrity through DNA replication, repair, and recombination by interacting with a variety of proteins associated with DNA repair and telomere maintenance. The accelerated aging associated with WS is reportedly caused by telomere dysfunction, and the underlying mechanism of the disease is yet to be elucidated. Although it was reported that the life expectancy for patients with WS has improved over the last two decades, definitive therapy for these patients has not seen much development. Severe symptoms of the disease, such as leg ulcers, cause a significant decline in the quality of life in patients with WS. Therefore, the establishment of new therapeutic strategies for the disease is of utmost importance. Induced pluripotent stem cells (iPSCs) can be established by the introduction of several pluripotency genes, including *Oct3/4*, *Sox2*, *Klf4*, and *c-myc* into differentiated cells. iPSCs have the potential to differentiate into a variety of cell types that constitute the human body, and possess infinite proliferative capacity. Recent studies have reported the generation of iPSCs from the cells of patients with WS, and they have concluded that reprogramming represses premature senescence phenotypes in these cells. In this review, we summarize the findings of WS patient-specific iPSCs (WS iPSCs) and focus on the roles of telomere and telomerase in the maintenance of these cells. Finally, we discuss the potential use of WS iPSCs for clinical applications.

Keywords: Werner syndrome (WS), accelerated aging, chromosomal instability, telomere dysfunction, induced pluripotent stem cells (iPSCs), reprogramming, telomerase, premature senescence phenotypes

INTRODUCTION

Werner syndrome (WS) is a rare human autosomal recessive disorder characterized by early onset of aging-associated diseases, chromosomal instability, and cancer predisposition (Goto, 1997, 2000). Fibroblasts from patients with WS exhibit premature replicative senescence (Salk et al., 1981b). *WRN*, the gene responsible for the disease, encodes a RecQ-type DNA helicase (Oshima et al., 1996; Yu et al., 1996; Goto et al., 1997; Matsumoto et al., 1997) that is involved in the maintenance of chromosome integrity during DNA replication, repair, and recombination (Shimamoto et al., 2004; Rossi et al., 2010).

WRN is a member of the RecQ helicase gene family, and other members of the family include BLM and RTS/RECQL4, which are mutated in Bloom syndrome (BS) and Rothmund–Thomson syndrome (RTS), respectively (Ellis et al., 1995; Kitao et al., 1999). BS and RTS, along with WS, are characterized by chromosomal instability, due to which RecQ helicases are considered to be the guardian angels of the genome (Shimamoto et al., 2004; Bohr, 2008). There are five members in the RecQ helicase gene family, including RECQL1 (Seki et al., 1994) and RECQL5 (Kitao et al., 1998; Shimamoto et al., 2000), the mutations of which have yet to be identified in human diseases.

Major clinical symptoms of WS include common age-associated diseases, such as insulin-resistant diabetes mellitus, and atherosclerosis. Recent advances in drug therapy for these diseases are available and are known to increase the lifespan of patients with WS. However, there is no effective therapy for intractable features, such as severe skin ulcers leading to a decrease in quality of life (QOL), which is a serious problem in patients with WS. Thus, there is an urgent need to develop a new treatment strategy for this syndrome. Regenerative medicine, such as autologous cell transplantation, could be considered as one of the therapeutic strategies for WS, and a potential choice is the use of patient-specific iPSCs.

Somatic cell reprogramming follows the introduction of several pluripotency genes, including *Oct3/4*, *Sox2*, *Klf4*, *c-myc*, *Nanog*, and *Lin-28*, into differentiated cells such as dermal fibroblasts, blood cells, and others (Takahashi and Yamanaka, 2006; Takahashi et al., 2007; Yu et al., 2007; Aoi et al., 2008; Stadtfeld and Hochedlinger, 2010; Okita and Yamanaka, 2011). During reprogramming, somatic cell-specific genes are suppressed, while embryonic stem cell (ESC)-specific pluripotency genes are induced, leading to the generation of induced pluripotent stem cells (iPSCs) with undifferentiated states and pluripotency

(Stadtfeld et al., 2008). Somatic cell reprogramming generates iPSCs characterized by pluripotency and infinite proliferative potential similar to the ESCs, and this technology opens up new possibilities for tailor-made regenerative medicine (Stadtfeld and Hochedlinger, 2010; Okita and Yamanaka, 2011).

Recently, two groups reported the generation of iPSCs from the cells of patients with WS and came to the similar conclusion that reprogramming repressed premature senescence phenotypes in WS cells (Cheung et al., 2014; Shimamoto et al., 2014). They demonstrated the successful reprogramming of cells from patients with WS into iPSCs with restored telomere function and stable karyotypes, suggesting that the induction of the gene encoding human telomerase reverse transcriptase (hTERT) during reprogramming suppresses telomere dysfunction in WS cells lacking WRN. In this review, we summarize the findings of WS patient-specific iPSCs (WS iPSCs) reported in the literature, and focus on the roles of telomere and telomerase in maintenance of these cells. We also review the recent progress in the clinical management of WS and explore stem cell therapy as a new strategy for WS treatment. WS iPSCs will provide opportunities not only for a better understanding of the pathogenic processes and modeling of the complex features of WS, but also for drug screening as well as the discovery and development of a new strategy for its treatment.

FUNCTION OF WRN HELICASE

Prolonged S-phase and reduction in frequency of DNA replication initiation observed in WS cells have implicated the role of WRN helicase in DNA replication (Hanaoka et al., 1983; Poot et al., 1992). The fact that WRN helicase interacts with several factors involved in DNA replication, including RPA, PCNA, FEN-1, and Topoisomerase I, supports this theory (**Figure 1**; Shimamoto et al., 2004; Rossi et al., 2010). WS cells are hypersensitive to a Topoisomerase I inhibitor, camptothecin (Okada et al., 1998; Poot et al., 1999), and WRN nuclear foci induced by the DNA damage caused by camptothecin are co-localized with RPA in the S-phase (Sakamoto et al., 2001). In addition, WRN helicase forms or unwinds the Holliday junction intermediate associated with a regressed replication fork (Sharma et al., 2004; Machwe et al., 2007). These observations suggest that the WRN helicase is involved in the re-initiation of a stalled replication fork. WS cells also show hypersensitivity to 4NQO that induces oxidative damage (Gebhart et al., 1988). Since accumulation of oxidative DNA damage is associated with aging, it is suggested that the WRN helicase is associated with one of the oxidative repair mechanisms, base excision repair (BER), and is known to interact with BER factors, polδ, polβ, PCNA, RPA, FEN-1, and PARP-1 (**Figure 1**; Rossi et al., 2010). Furthermore, the WRN helicase unwinds a BER substrate produced by uracil-DNA glycosylase and AP endonuclease (Ahn et al., 2004). It is also known that the helicase interacts with the double-strand break repair factors Ku, DNA-PKcs, and the Mre11-Rad50-Nbs1 complex, as well as the telomeric DNA protecting proteins, TRF1, TRF2, and POT1 (**Figure 1**; Shimamoto et al., 2004; Rossi et al., 2010). Additionally, Tahara et al. (1997) reported abnormal telomere dynamics in WS lymphoblastoid cell lines (LCLs) with weak or no telomerase activity. These findings suggest that the WRN helicase is involved in telomere metabolism. WRN helicase is shown to resolve Holliday junctions (Sharma et al., 2004), G-quadruplexes formed in telomere G-rich sequences (Mohaghegh et al., 2001), and higher-ordered DNA structures, such as the D-loop (Opresko et al., 2004). These DNA structures formed at telomere ends must be resolved during DNA replication to be accessible to DNA polymerases and telomerase, therefore, WRN helicase might function in the resolution of higher order structures in telomeric DNA.

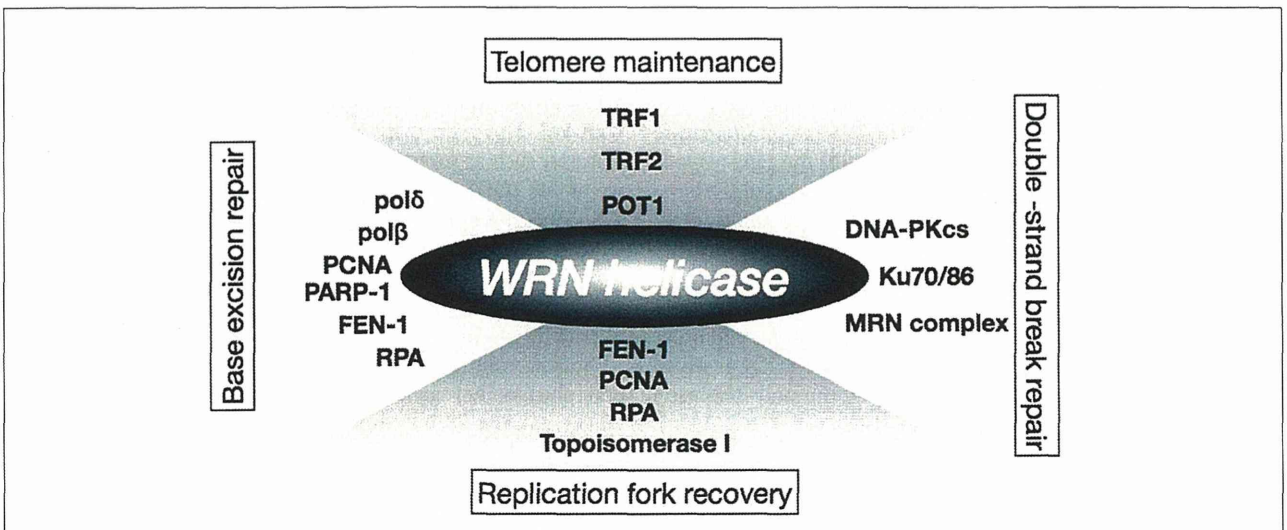

FIGURE 1 | Function of WRN helicase. WRN helicase functions through interaction with factors involved in replication (RPA, PCNA, FEN-1, Topoisomerase I), base excision repair (BER; polδ, polβ, PCNA, RPA, FEN-1, PARP-1), double-strand break repair (Ku, DNA-PKcs, Mre11-Rad50-Nbs1 complex), and telomere maintenance, (TRF1, TRF2, POT1).